Available online at www.sciencedirect.com

ScienceDirect

Ceramics International 40 (2014) 4953–4962

CERAMICS INTERNATIONAL

www.elsevier.com/locate/ceramint

SiO_2 nanoparticles addition effect on microstructure and pinning properties in $YBa_2Cu_3O_y$

M.K. Ben Salem[a,*], E. Hannachi[a], Y. Slimani[a], A. Hamrita[a], M. Zouaoui[a], L. Bessais[b], M. Ben Salem[a], F. Ben Azzouz[a,c]

[a]*L3M, Department of Physics, Faculty of Sciences of Bizerte, University of Carthage, 7021 Zarzouna, Tunisia*
[b]*CNRS-ICMPE-UMR 7182, University of Paris 12, Paris, France*
[c]*College of Sciences-Girls, University of Dammam, Dammam, Saudi Arabia*

Received 17 July 2013; received in revised form 17 October 2013; accepted 20 October 2013
Available online 30 October 2013

Abstract

A series of $YBa_2Cu_3O_y$ (YBCO, Y-123) samples with small amounts (0–1 wt%) of nanosized SiO_2 particles (30 nm) are synthesized in air using a solid-state reaction route. The microstructure has been characterized by transmission and scanning electron microscopy (TEM and SEM) techniques and the magnetic field and temperature dependences of the critical current density (J_c) was calculated from the magnetization measurements and by the standard four-probe method at various temperatures. Flux pinning force density (F_p) is calculated and possibility of the pinning mechanisms prevalent in type II superconductors are investigated. X-ray diffraction analysis shows that the orthorhombic structure of YBCO is maintained. Morphology examination by SEM revealed decreases of grain size with SiO_2 addition. High zero resistance temperature T_{co} value of about 90 K was maintained in YBCO with SiO_2 concentration ≤ 0.2 wt%. Compared to free added-sample, higher critical current densities were obtained for the YBCO sintered with low concentration SiO_2 (≤ 0.1 wt%) in applied magnetic field. TEM observations show the presence of columnar defects (2–3 nm in diameter) along the *c*-axis of YBCO and Si-rich nanophase embedded in the superconducting matrix. These defects are responsible for critical current densities improvement in the magnetic field of YBCO.

Keywords: YBCO superconductor; SiO_2 nanometer; Microstructure; Critical currents; Flux pinning

1. Introduction

Following the discovery of type-II high-temperature superconductors, work has proceeded to develop these materials for power applications. One of the problems, however, has been that magnetic flux is not completely expelled, but rather is contained within magnetic fluxions, whose motion prevents larger supercurrents. For polycrystalline samples, the intergranular critical current density is limited by weak links caused by grains boundaries and the intra-granular critical current is impeded principally by the thermally activated flux flow at high temperatures and applied magnetic fields. For applied magnetic fields higher than B_{c1} (B_{c1}, the lower critical field), the flux motion in granular high temperature superconductors (HTS) samples cannot be completely understood by considering the vortices in the inter-grain and intra-grain independently. To prevent the vortex motions and enhance the flux pinning strength it is necessary to introduce artificial pinning centers (APCs) in a superconductor apart from those which occur naturally [1–8]. These APCs can be described as one-dimensional (1D) such as dislocations, two-dimensional (2D) such as grain boundaries and three-dimensional (3D) such as fine precipitates. Various techniques such as high energy ion irradiation [9], high energy ball milling [10], chemical doping and additives [11,12] have been reported in the literature to act as artificial pinning centers. The route of artificially introducing inhomogeneities or secondary phase materials as flux pinning sites in HTC is an effective method and more practical

*Corresponding author. Tel.: +21 67 259 1906; fax: +21 67 259 0566.
E-mail addresses: salemwiem2005@yahoo.fr, mohamed.bensalem@fsb.rnu.tn (M.K. Ben Salem).

0272-8842/$ - see front matter © 2013 Elsevier Ltd and Techna Group S.r.l. All rights reserved.
http://dx.doi.org/10.1016/j.ceramint.2013.10.103

compared to physical techniques. Various kinds of oxide doping and additives, including metal [13] nonmetal nanoparticles [4,5,14] and carbon nano-tubes [12] have shown positive effects on critical current densities in HTC. Presently, oxide perevoskites ($BaZrO_3$, $BaSnO_3$, $BaNb_2O_3$, etc.) nano-additives have garnered the most interest as a class of materials for incorporation into YBCO. These additives improve the pinning ability by forming composites or acting as column defects comprised of self-alighted nanostructure such as nanodots and nanorods [15–17]. In the present study we demonstrate that nanosized SiO_2 particles addition can generate also columnar defects in YBCO.

The impact of Si-based nanomaterials addition on the superconducting properties of HTC has already been studied in earlier years but most of them are focused on the MgB_2 superconductor materials [18–23]. The effects of Si-based nanomaterials in HTC ceramics other than MgB_2 remain inconclusive and opposite results were reported. Therefore for an accurate validation of the impact of those materials further studies would be required. Nanoparticles of SiC and SiO_2 imparted modifications in the microstructural and an enhancement of pinning properties for MgB_2. The above nanoadditives do not affect the MgB_2 phase formation for suitable concentration levels. The zero resistance temperature (T_{co}) decreases slightly, and the critical current density under applied magnetic field ($J_c(H)$), the irreversibility magnetic field (H_{irr}) characteristics have been significantly improved. Guo et al. [20] reported on the effect of nanosized SiC addition on polycrystalline Bi-2223 and they found that a small amount of SiC (0.15 wt%) improved the critical current I_c and its behavior in magnetic field as a result of the enhancement in density, grain alignment, grain connectivity and flux pinning of samples. However, larger Si-based nanoadditive concentrations inhibit the formation of the high-Tc phase and decrease J_c. Nanosized SiO_2 addition shows a negative effect on T_{co} and J_c of $SmBa_2Cu_3O_7$ materials due to the reaction between SiO_2 and matrix. [22]. Moreover, the substitution of small amounts of Si at Cu sites in CuO_2 planes has been found to suppress the superconductivity in cuprate systems such as $(Cu_{0.5},Tl_{0.5})Ba_2Ca_2Cu_3O_{10-d}$ [23]. Although research has been performed on the effect of nanosized Si-based materials on some HTC superconductors, no data have been published regarding this effect in YBCO. For YBCO, SiO_2 generally used as a substrate to synthesize YBCO film, which leads to a significant degradation of superconducting properties caused by the interdiffusion of Si due to high substrate temperature during the deposition [24]. However, experimental results of ageing tests showed that SiO_2 layer forms an excellent passivation material for preventing YBCO from corrosion by water [25]. To our knowledge there is only one work devoted to the YBCO reporting the effect of SiO_2 powder addition during the initial sintering cycles on the superconducting properties of YBCO [26]. Structural analyses show that SiO_2 addition leaving the Y-123 structure practically intact but influences the inter-grain regions of the $(YBa_2Cu_3O_{7-d})_{1-x}/(SiO_2)_x$ composite samples. The magnetoresistivity and isothermal magnetization (M–H) measurements were explored and demonstrate that SiO_2 degrades the width of the M–H loops and the H_{irr} and strongly affects the flux dynamics determined by the inter-grain regions of the samples. Accordingly, based on scanning electron microscopy observations, they have assumed that small particles of SiO_2 are sticking on the surface of the YBCO grains. In the present work we demonstrate that nanosized SiO_2 particles addition effectively controlled the micro-structure development in YBCO and hence the superconducting properties like $J_c(H)$, $J_c(T)$, F_p.

Moreover, the common point between different cited reports is that a suitable amount of nanosized SiO_2 particles does not affect the formation of superconducting phase and not alter T_{co}. So this additive satisfies useful criteria to design a composite superconductor-nonsuperconductor with better physical and mechanical properties. With this objective in mind, we performed SiO_2 nanometer sized particle doping experiments, investigating the influence of the SiO_2 addition during the final sintering cycles of YBCO on the microstructural features and the superconducting properties like J_c, pinning force density F_p, which are useful in practical applications of these materials. Nano-material additives may thus be more efficient during the final sintering cycles of YBCO superconductor, which adjust the local microstructure by generating defects such as twin boundaries, inhomogeneous microdefects, dislocations, columnar defects, stacking faults, oxygen vacancies, impurity phases, precipitates, and poor superconducting phase etc. As a consequence of both the unavoidability and desirability of defects in the oxide superconductors, investigation by TEM is required to determine the local microstructure; i.e., to detect deviations from the average microstructure, determined by SEM.

The investigation of the pinning properties in superconductors is usually accomplished by the determination of the flux pinning force densities, $F_p = J_c \times \mu_o H$. The pinning force of superconductors is a function of temperature and magnetic field and is determined by the micro and nanostructure of the sample. F_p is mainly depends on the pinning center size, which determines the total length of interacting flux lines, and the geometrical nature of the interaction. Because of the complexity of defects in polycrystalline superconductors, more than one type of pinning mechanism may exist in high-Tc superconductors and the effects of the different types of mechanisms may be additive. It is an important task to find the dominant ones.

To provide more evidence concerning the effect of SiO_2 nanoparticles inclusion on the superconducting properties of YBCO ceramics, a series of specimens with different amounts of SiO_2 (0–1.0 wt%) addition were prepared by two steps solid-state reaction method. In this paper, we present our experiments and results on the superconducting properties and the changes in microstructure correlated with nanosized SiO_2 addition and the pinning mechanisms. The magnetic field and the temperature dependences of the critical current have been studied with a central objective to determine the dominant source and mechanism of vortex pinning. The pinning force densities were analyzed using the Dew–Hughes model [27] and the microstructure was examined using TEM technique.

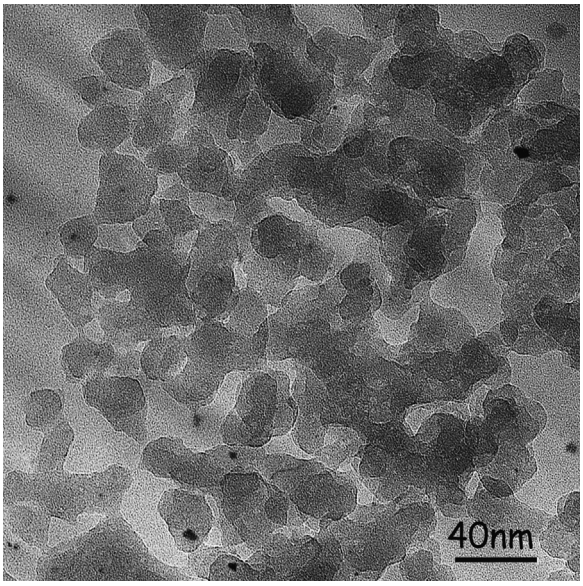

Fig. 1. TEM micrograph of SiO_2 nanoparticles.

We establish that nanosized SiO_2 addition particles effectively controlled the micro-structure development in YBCO and hence the superconducting properties.

2. Experimental

The pure and SiO_2 nanoparticles added YBCO samples were prepared by the conventional solid-state reaction method under identical conditions. The single phase YBCO was synthesized by thoroughly mixing high purity Y_2O_3 (99.9%), Ba_2CO_3 (99.9%) and CuO (99.9%) according to the chemical formula of Y:Ba:Cu = 1:2:3. This mixture of powders was pelletized and then calcined at 950 °C for 12 h in air in order to produce an oxide precursor without remainder of any carbonates. X-ray diffraction revealed that YBCO powder was thus elaborated with a main phase composition of Y-123. SiO_2 nanoparticles were added to the precursor powder Y-123 in the final processing stage, by mixing and hand grinding both powders in an agate mortar. Fig. 1 shows transmission electron microscopy image of the SiO_2 which was used as an additif. The average size of the SiO_2 nanoparticles was about 30 nm in diameter. The additional amount of SiO_2, varied from $x=0$ to $x=1$ wt% of the total mass of sample. The mixed powders were pressed into pellets at 750 MPa in the form of circular disks having 13 mm in diameter. The pellets were sintered at 950 °C for 8 h in air and, then, cooled to room temperature at a rate of 4 °C/min. The heat treatment processes of all samples were performed in alumina crucibles. The non added powder (0 wt%) was used as a reference, then it is hand ground as the SiO_2 added samples to ensure identical physical conditions for all the samples.

The structure and phase identification of the powder sample ground from sintered pellets were examined by powder X-ray diffraction (XRD) using a Philips 1710 diffractometer with Cu$K\alpha$ radiation. The diffraction data were collected over the diffraction angle range of $2\theta = 10°–100°$ by step scanning with a width of 0.015° and a scanning step time of 10 s. The microstructure of samples was characterized using FEI Nano Lab 200 scanning microscopy and FEI Tecnai *G*2 transmission electron microscopy operating at 200 kV with a LaB_6 filament. Local chemical analysis was performed using the energy dispersive X-ray spectroscopy (EDXS) system attached to the TEM. The transport properties of the samples were studied by measuring the electrical resistivity-temperature $\rho(T)$ and current–voltage (I–V) characteristics using the four-probe technique. For electrical measurements the pellets were carefully cut into rectangular bar shaped samples with almost similar dimensions and with active cross-sections for current flow of 0.6 mm^2. Electrical contacts were made using silver paint and the contact resistance value was approximately 0.5 Ω. The temperature dependence of the electrical resistivity ρ(T) was measured using DMX-19 SCC cryostat system. The magnitude of the excitation current of density $J = 40$ μA/cm^2 was used to measure resistivity of the samples. The transport critical current density (J_{ct}) values were determined at various temperatures using a 5 μV/cm criterion and the excitation current was injected along the length of the samples. The isothermal magnetization (M–H) of the samples was measured by using a Quantum Design Physical Properties Measurement System (PPMS9) at various temperatures in magnetic fields up to 6 T. The sample was mounted such as that its wide surface was along the direction of the magnetic field. The intragrain critical current density (J_{cm}) was determined from the hysteresis width of the magnetization measurement using the extended Bean model [28].

3. Results and discussion

Fig. 2 shows the powder XRD patterns of nanoparticles SiO_2 added YBCO samples. The analysis of the data indicates a predominantly single phase perovskite structure Y-123 with orthorhombic Pmmm symmetry. No orthorhombic- tetragonal phase transition was detected up to $x=1$ wt% under the accuracy of XRD patterns. Thus it seems that SiO_2 does not enter the Y-123 structure. For higher SiO_2 amount (1 wt%),

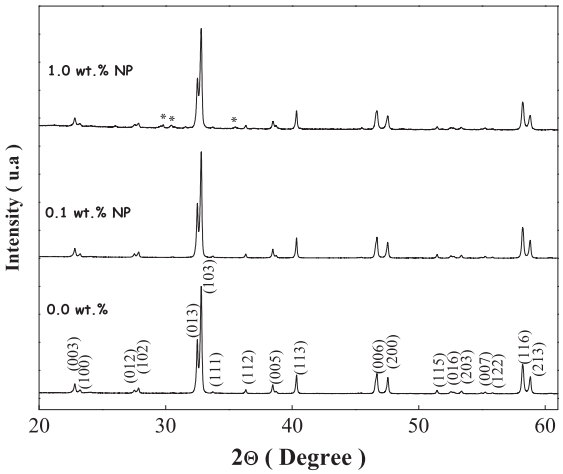

Fig. 2. X-ray powder diffraction patterns of samples added with various amounts of SiO_2 nanoparticles. *: Y_2BaCuO_5.

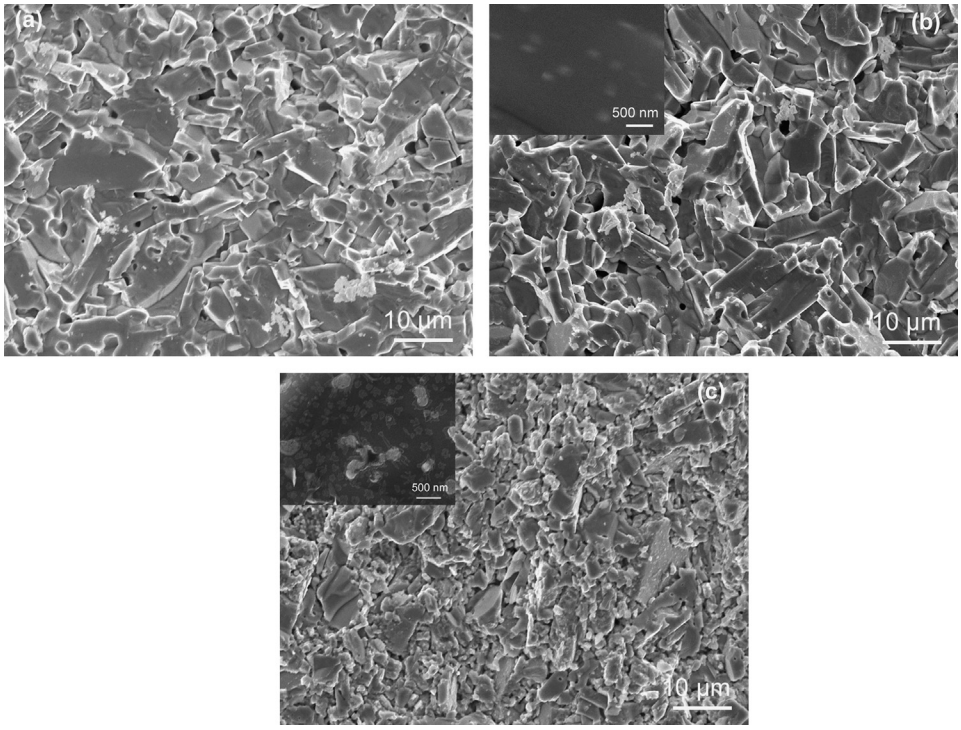

Fig. 3. SEM micrographs of samples added with nano-sized SiO_2 particles: (a) non-added, (b) with 0.1 wt%, and (c) with 1 wt%. Insets: high magnification SEM micrograph showing Si-rich particles embedded in the YBCO grains.

SiO_2 peaks with very low intensity and a small quantities of Y_2BaCuO_5 secondary phase were detected. The XRD patterns were analyzed by the Rietveld structure refinement method. The R_p and R_{wp} factors and the goodness of fitting were used as the numerical criteria of fitting. It may noticed that a, b and c lattice parameters remain almost constants with SiO_2 addition. The measured lattice parameters are $a=0.3817$ nm, $b=0.3882$ nm, $c=1.1674$ nm with an estimated 0.0001 nm precision. The oxygen stoichiometry as deduced from the oxygen occupancy factor remains almost constant for all samples. Samples remained orthorhombic, with the distortion $(b-a)/(a+b)$ very close to the that of pristine sample (8.510^{-3}). The orthorhombic structure can be visualized with the help of characteristic orthorhombic splitting of reflections (0 1 2), (1 0 2) and (0 1 3), (1 0 3). Hence, any phenomenon that may occur in this study is assumed to be irrelevant to the structure change of these YBCO samples.

The SEM micrographs of wide surface morphologies of free, 0.1 and 1 wt% SiO_2 nanoparticles added samples are respectively shown in Fig. 3a–c. The microstructure of samples exhibits a granular structure with a dominant YBCO phase. The average grain size decreases for increasing SiO_2 content. The decreasing of grain size has been reported in the case of Ca doped YBCO system [29]. A closer look with higher magnification (inset of Fig. 3b and c) for SiO_2 nanoparticles added samples shows the presence of almost regular form of nanometer scale entities bright in contrast with average size around 200 nm. These entities take place into grains along with some segregation in the grain boundaries. The density of these entities increases with increasing SiO_2 concentration. Such entities were not observed in free added sample. EDXS analyses performed on areas with nanometer scale particle entities show the presence of Si element.

In order to obtain more detailed information of the microstructure of nanoparticles SiO_2 added samples, we performed transmission electron microscopy. Fig. 4a shows TEM micrograph taken along the [1 0 0] axis of YBCO. This figure shows the presence of nanophases incorporated within the YBCO matrix. EDXS analyses collected from these nanophases show the presence of silicon (Fig. 4c). Nanosized entities embedded in YBCO worked as isotropic pinning centers and enhanced the critical current density in magnetic fields. Additionally, uninterrupted columnar defects aligned along the c-axis of the YBCO are clearly observed. The diameter of this defect is estimated to be on the order of 2–3 nm (Fig. 4b). Such columnar defects have been observed in the case of YBCO irradiated by high energy heavy ion [30]. Columnar defects were proven to be efficient pinning centers in HTSC compounds [31]. It seems that these columnar defects are caused by the presence of Si-rich nanophases but the formation mechanism of these columnar defects is not clear. Interrupted columnar defects comprised of self-aligned $BaZrO_3$ and $BaSnO_3$ nanodots of 3–10 nm parallel to the c-axis of the YBCO layers are reported in the literature [15,16]. It is expected that columnar defects work as c-axis correlated pinning centers so the extension of the straight portion is very important to obtain a large pinning.

Measurements of the resistivity dependence on the temperature ($\rho(T)$) for different samples with various amounts of SiO_2 nanoparticles are shown in Fig. 5. As can be seen from this

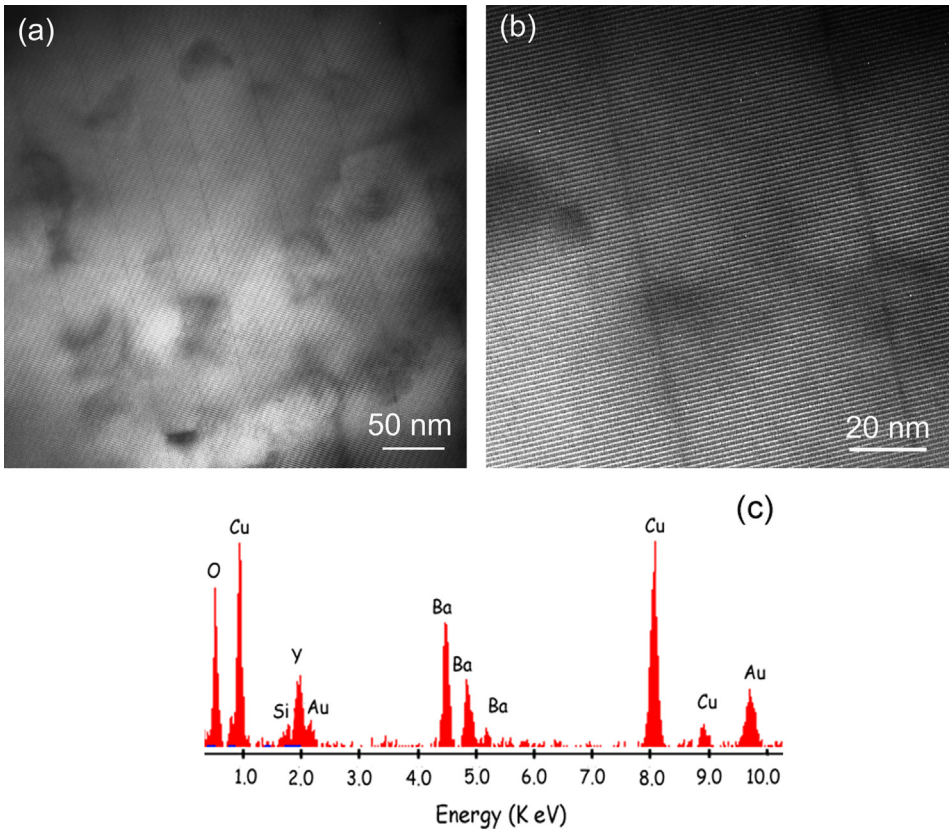

Fig. 4. ((a) and (b)) TEM micrographs of SiO_2 added sample showing inhomeginities inclusions in the YBCO matrix and columnar defects. (c) EDXS spectrum taken from the area with nanoscale entities.

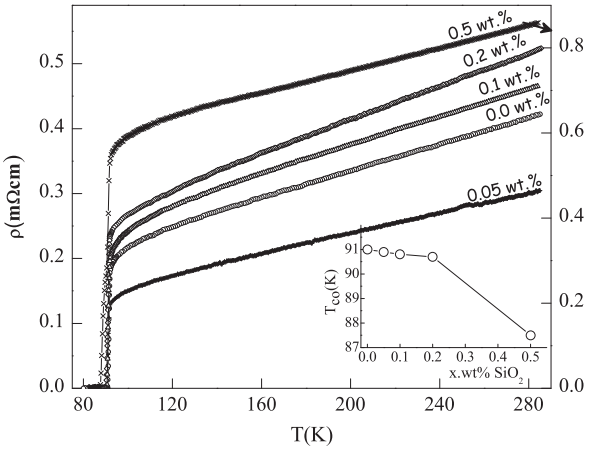

Fig. 5. Resistivity dependence on the temperature for samples added with various amounts of SiO_2 nanoparticles. Inset: Evolutions of the zero-resistivity temperature T_{co} of samples sintered with different amounts of SiO_2.

figure, all samples show a metallic behavior in the normal state and a superconducting transition to zero resistance. The absolute resistivity in the normal state depends on porosity, grain boundaries scattering etc., and its linearity for longer temperature interval confirms the idea that the preparation and synthesis of samples procedure are done correctly, with optimal value of oxygen content. The 0.05 wt% SiO_2 added sample exhibits the lower normal-state resistivity and residual resistivity ρ_o.ρ_o is obtained from the fitting of resistivity data in the temperature range 140 K $\leq T \leq$ 285 K by the linear equation: $\rho(T)=\rho_o+\alpha T$. This implies that the disorder, the porosity and the impurity scattering in the CuO_2-plane in this sample are the lowest. For lower SiO_2 added samples the slope α of the $\rho(T)$ in the normal state does not show an appreciable change, however, for higher SiO_2 concentration $\rho(T)$get flatter in shape. Inset of Fig. 5 reports the zero resistance temperature, T_{co}, for YBCO with different amounts of SiO_2 nanoparticles. T_{co} value of about 91 K was maintained in YBCO bulks with SiO_2 concentration $\leq$0.2 wt%. With increasing SiO_2 content no change is observed in the onset temperature of the superconducting transition (T_c^{onset}close to 93 K), whereas, the temperature at which $\rho(T)$ goes to zero is found to show a tail. The observation of an almost constant value of T_c^{onset} in all samples suggests that the grains in these samples are not affected by the presence of SiO_2. This is in excellent agreement with the XRD results which demonstrate no change in XRD peak positions of Y-123 phase. The zero resistivity temperature, T_{co}, is slightly depressed by introducing low concentration of SiO_2 nanoparticles indicating that there are little effects of SiO_2 on the YBCO bulk.

Measurements of the global transport critical current density, J_{ct}, at 77 K under self magnetic field for samples sintered with various amounts of SiO_2 are shown in Fig. 6a. It is clear that the addition of a small amount of SiO_2 ($\leq$0.1 wt%) enhances the current-carrying capacity of YBCO ceramics, however, a larger amount of SiO_2 decreased the current-

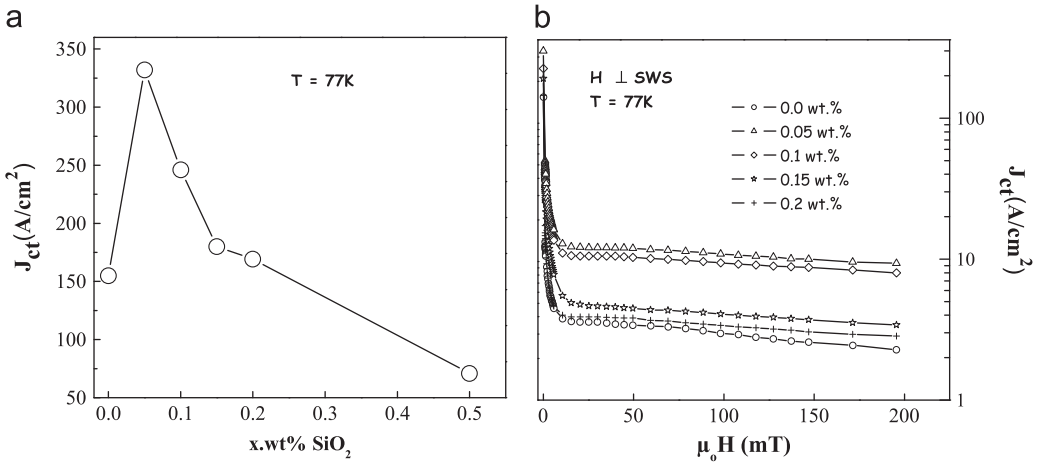

Fig. 6. (a) Transport critical current densities at 77 K under self magnetic field and (b) under various applied magnetic field of samples added with various amounts of SiO_2 nanoparticles. Magnetic field was applied perpendicular to the samples wide surface.

carrying capacity compared to the free added sample. These J_{ct} values are interesting for all samples, especially when compared to the values reported in the literature in the case of $YBa_2Cu_3O_y$, doped with Ag nanoparticle [13] with Zr [32] and $Y_{1-x}Ca_xBa_2Cu_3O_z$ [33] polycrystalline samples. There is an increase in J_{ct} of about 200% for the 0.05 wt% SiO_2 added sample. In order to clarify the effect of SiO_2 nanoparticles addition on the flux pinning properties, we measured J_{ct} of samples under magnetic field. Based on the results of the J_{ct} measurements we have chosen samples sintered with SiO_2 concentrations ≤ 0.2 wt%. Fig. 6b shows the dependence of critical current densities with magnetic field, $J_{ct}(H)$, applied along the sample wide surface (SWS). Compared to the pure YBCO sample, the SiO_2 added ones have much slower $J_{ct}(H)$ drops for applied fields. Throughout the whole range of applied magnetic field J_{ct} is increased by a factor of 3–4 times for samples sintered with SiO_2 concentration ≤ 0.1 wt%. The characteristic behavior of critical current density under applied magnetic field may come from the counterbalance of two effects simultaneously caused by SiO_2 addition. One effect is the formation of the efficient pinning centers which lead to the enhancement of pinning and the other effect is the decrease of T_c. In order to compare the relevant SiO_2 effect, we examined the temperature dependences of J_{ct} in applied magnetic field for free and 0.1 wt% SiO_2 added samples for example (Fig. 7). The 0.1 wt% SiO_2 added sample shows higher $J_{ct}(H)$ than the pure one throughout the considered whole range of temperature. Fig. 8 displays the $J_{ct}(H)$ of 0 and 0.1 wt% SiO_2 added samples measured at 77 K for applied either parallel (i.e., H// SWS) and perpendicular (i.e., H⊥SWS) to the sample wide surface. For both magnetic field directions, the J_{ct} of 0.1 wt% SiO_2 added sample is the best. When the direction of the applied field is parallel to SWS, a smoother decrease in J_{ct} is observed. We note that the difference between the $J_{ct}(H//SWS)$ and $J_{ct}(H\perp SWS)$ is less significant in the case of the SiO_2 added sample. The ratio $J_{ct}(H//SWS)/J_{ct}(H\perp SWS)$ is estimated and the obtained values are about 1.6 and 1.3 for free and added samples respectively. As revealed by TEM columnar defects and uniformly dispersed nanophases and other generated defects which act as pinning centers result in an overall enhancement in the flux pinning as well as reduced $J_{ct}(H)$ anisotropy of SiO_2 added sample. It is reported that the columnar defects (functionalizing as 1-D APCs) aligned along the c-axis of YBCO films worked as anisotropic pinning centers and enhanced the critical current density values in the magnetic fields applied parallel to c-axis of the YBCO films [34]. Indeed, when the direction of the magnetic field is tilted from the direction of columnar defects a zigzag state of the vortex line comes to stabilize in energy and the pinned portion of vortex is shortened and as consequence the vortex line comes free from the columnar defects by a small variation of Lorentz force, leading to the decrease of critical current density [35]. Moreover, polycrystalline superconductor materials can be regarded as a distribution of YBCO crystallites with random orientations, thus at each direction of the applied magnetic field, it is possible to find columnar defects parallel to the vortex line.

To obtain further insights of the intragranular pinning we have estimated the field dependence of critical current density, $J_{cm}(H)$, determined from magnetic hysteresis loops measured at various temperatures for free and 0.05 wt% added samples. The J_{cm} values were estimated according to the extended Bean model [28] by using the following equation:$J_{cm} = 20(\Delta M)/a(1-a/3b)$, ΔM is the magnetization hysteresis, a and b are the cross-sectional dimensions of the sample perpendicular to the applied field and $a < b$. Fig. 9 presents the magnetic field dependences $J_{cm}(H)$ of free and 0.05 wt% SiO_2 added samples. The obtained result shows that the SiO_2 additive reduces the sensitivity to the magnetic field. SiO_2 added sample shows a distinctly higher J_{cm} for all the temperature range if compared to the virgin sample. Throughout the whole range of applied magnetic field, factors of ~ 1.4 to 1.6 in J_{cm} improvements was observed for SiO_2 added sample compared to that of free one when the temperature decreases from 77 to 20 K. Earlier works on the chemical doped bulk samples prepared by solid state reaction method

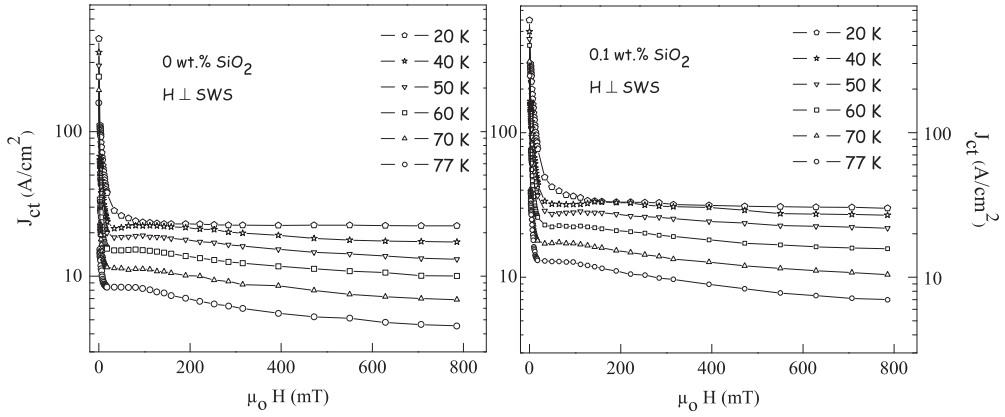

Fig. 7. Magnetic field dependence of the transport critical current densities measured at various temperature for free and 0.1 wt% added-samples. Magnetic field was applied perpendicular to the samples wide surface.

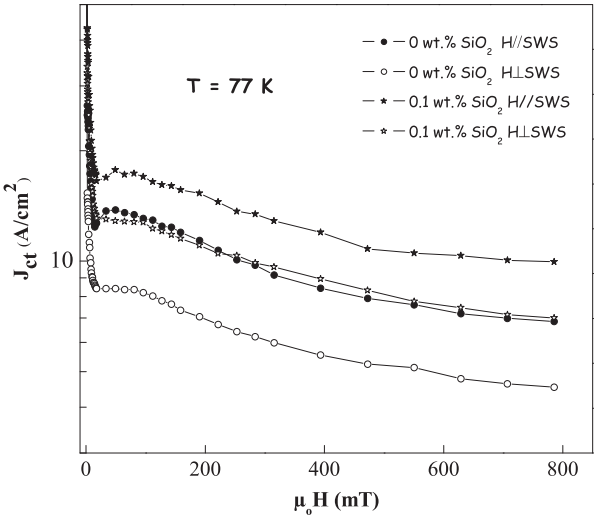

Fig. 8. Comparison of critical current densities dependence on magnetic field at 77 K for free and 0.1 wt% added samples. Magnetic field was applied parallel and perpendicular to the sample wide surface.

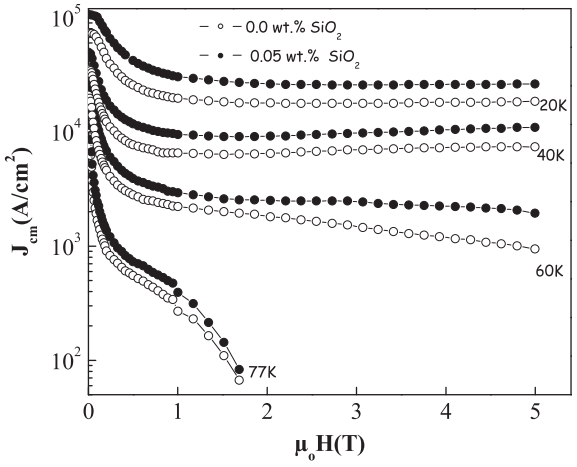

Fig. 9. Critical current density J_{cm} calculated by magnetization loops versus magnetic field at various temperature for free and 0.05 wt% SiO_2 added samples.

showed a lesser enhancement of critical current density; a factors of about 1.2 in J_{cm} improvements was reported at applied field of 1 T [36].

In order to determine the strength of the pinning centers involved in each contribution and classify them into weak pinning (WP) and strong pinning (SP) we have compared the critical current densities using the theoretical predictions for weak [37] and strong-correlated [38] vortex pinning given by:

$$J_c^{WP}(T) = J_c^{WP}(0)\exp(-T/To) \quad (1)$$

$$J_c^{SP}(T) = J_c^{SP}(0)\exp(-3(T/T^*)^2) \quad (2)$$

where $J_c^{WP}(0)$ and $J_c^{SP}(0)$ are the critical current densities at 0 K for weak and strong pinning contributions respectively, and T_o and T^* are characteristic temperatures which fix the energy scale of the pinning centers for each contribution. The weak pinning centers are mainly due to the defects associated to the nanophase embedded in the YBCO matrix and strong-correlated disorder where strong pinning occurs are due to the columnar defects, twins in YBCO single crystals [38] and the superconducting/nanophase interface [6–39]. The measured self-field temperature dependence of the critical current density of SiO_2 added YBCO sample should account for the sum of the weak and strong pinning contributions. Fig. 10, shows a comparison of the experimental data of the temperature dependence of the critical current density measured in the self-field of the free and SiO_2 added samples and the fitted profiles considering the sum of the pinning contributions (solid lines). First of all, a comparison between samples shows that the critical current density of the added sample has increased for all temperatures if compared to the virgin sample. We have also fitted the experimental data by considering separate contributions of weak and strong pinning centers. Results are shown in Fig. 10; dashed and dash-dot curves represent respectively the fits based on Eqs. (1) and (2). Notice that weak pinning centers are dominant at low temperatures ($T < 30$ K) and at higher temperatures the strong pinning centers contribution dominates. It can be noted that $J_c^{WP}(0)$ and $J_c^{SP}(0)$ are modified by the addition of SiO_2 nanoparticles

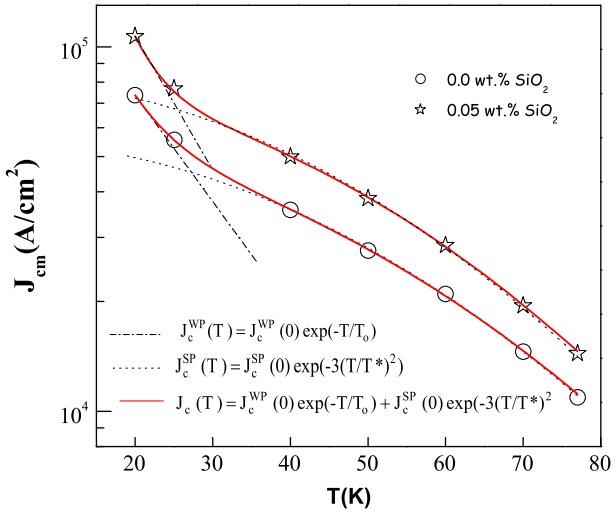

Fig. 10. Temperature dependence of the self-field critical current density J_{cm} for free and 0.05 wt% added samples. The lines correspond to the fit of the experimental data by using Eqs. (1) and (2) in the text.

in the YBCO matrix. $J_c^{WP}(0)$ and $J_c^{SP}(0)$ increase respectively by about 430% and 150% in the added sample as compared to the virgin one. If we correlate the microstructure with the improvement in the critical density in the added sample, two possible arguments can be speculated, one due to the Si-rich nanophase embedded in the superconducting matrix and the second one would be due to an increased pinning strength produced by columnar defects. Low content SiO_2 addition is able to introduce effective pinning centers without inducing any noticeable suppression of T_{co}, it is an effective way of enhancing bulks critical current density.

In order to obtain deeper inside into the origin of improved pinning properties with SiO_2 added samples an extended analysis of pinning force density is carried out. The pinning force density is calculated as $F_p = \mu_o J_{cm} \times H$ from measurements of the magnetic critical current density. Fig. 11a shows the flux pinning force density for free and 0.05 wt% SiO_2 added samples at 77 K. Clearly there is an increase in the pinning force with a small addition of SiO_2. The maximum values of the pinning force density, $F_{p\,\max}$, shifts to higher magnetic field. This supports our conclusion that the flux pinning strength of Y-123 increases with the addition of SiO_2.

The pinning force density, F_p, is mainly determined by the pinning center size because the pinning center size determines the total length of interacting flux lines, and the geometrical nature of the interaction. Compared to the inter-flux-line spacing, d, point pins, surface (line) pins and volume pins were considered. Dew–Hughes [27] proposed a general expression for the pinning force density for one type of pinning center i: $F_{pi}(h) = a_i h^{pi}(1-h)^{qi}$, where a_i is a numerical parameter independent of the applied field, h is the reduced magnetic field and (p_i,q_i) are parameters describing the actual pinning mechanism. In this model, there are six different pinning functions describing the core pinning using the general expression of F_{pi}: (1)$p = 0, q = 2$: normal, volume pinning; (2)$p = 1, q = 1$:$\Delta\kappa$-pinning, volume pins; (3) $p = 1/2$, $q = 2$: normal surface (line) pins; (4)$p = 3/2$, $q = 1$:$\Delta\kappa$-pinning, surface pins; (5)$p = 1$, $q = 2$: normal point pins; and (6) $p = 2$, $q = 1$: $\Delta\kappa$-pinning, point pins. The Dew–Hughes model is a direct summation of elementary pinning forces and the total pinning force density can be written as $F_p = \sum_{i=1}^{i=6} a_i h^{pi}(1-h)^{qi}$. Normalized pinning force density, $f_p = F_p/F_{p\,\max}$ is often scaled with $h = H/H_{irr}$, H_{irr} can be defined as the field at which $J_c(H)/J_c(0) = 10^{-3}$. In Fig. 11b, the plots of the f_p versus h are shown for free and 0.05 wt% added samples. For both samples, the large curves obtained indicate that the pinning properties cannot be explained by only one pinning mechanism over the whole region of h, which implies that more than one type of pinning source may be present at the same time. A fitting procedure using the Dew–Hughes model was performed for both samples. The experimental data produce a good fit as shown by the solid lines in Fig. 11b. For the free added sample, flux pinning curves accord with the surface (line)-like pinning of the normal phase and volume-like pinning of $\Delta\kappa$. For 0.05 wt% SiO_2 added sample, in addition to the mechanisms obtained in the free sample, volume pinning center of the normal phase comes to contribute to the total pinning. Moreover, the above results lead us to conclude that nanosized SiO_2 particles addition widens the normal phase embedded in superconducting material, and strengthens the normal pinning centers.

4. Conclusion

The effect of nano-sized SiO_2 particles (30 nm) addition on the superconducting properties of polycrystalline $YBa_2Cu_3O_y$ compounds was systematically studied. Samples were synthesized in air using a standard solid state reaction by adding nanosized particles up to 1 wt%. XRD analysis shows a predominantly single-phase perovskite structure with orthorhombic Pmmm symmetry. Morphology examination with SEM revealed a decrease of grain size with SiO_2 additions and Si-rich particle agglomerations distributed between YBCO grains in the samples sintered with higher nano-sized particles content. High T_{co}value of about 90 K was maintained in YBCO bulks with SiO_2 concentration ≤ 0.2 wt%. Critical current densities were investigated by magnetization (J_{cm}) and transport measurements (J_{ct}) under applied magnetic field at various temperature. Compared to free added-sample high critical current densities were obtained for the YBCO bulk sintered with low concentration of SiO_2 (≤ 0.1 wt%) in applied magnetic field. TEM observations show the presence of columnar defects (2–3 nm in diameter) along the c-axis of YBCO and Si-rich nanophase embedded in the superconducting matrix. These defects are believed to be responsible for critical current densities improvement in the magnetic field of YBCO bulks at various temperatures. From the temperature dependence of the critical currents we have separated two pinning centre contributions: weak and strong pinning centres. SiO_2 addition widens the normal phase embedded in superconducting material, and strengthens the normal pinning centers. The crux of this investigation is that with an addition nanosized SiO_2 particles during the final sintering cycles of

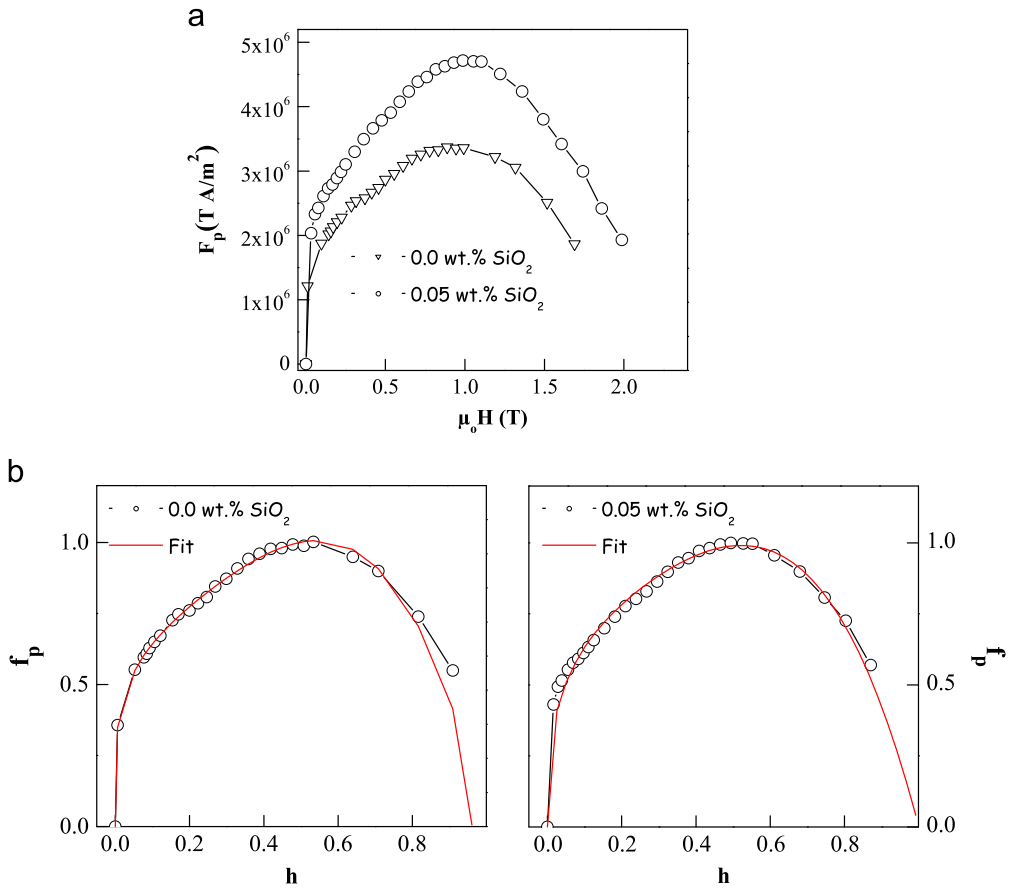

Fig. 11. (a) Magnetic field dependencies of flux pinning force density for free and 0.05 wt% SiO_2 added samples, (b) scaling of normalized pinning force versus reduced magnetic field; solid lines represent the theoretical curve according to the Dew–Hughes model.

YBCO, there is a significant improvement of superconducting properties like critical current density, pinning force density without alteration of zero resistive temperature of YBCO bulk polycrystalline samples.

References

[1] T. Matsushita, Flux pinning in superconducting 123 materials, Supercond. Sci. Technol. 13 (2000) 730.

[2] D. Larbalestier, A Gurevich, D.M. Feldmann, A. Polyanski, High-Tc superconducting materials for electric power applications, Nature 414 (2001) 368.

[3] R. Goswami, T.J. Haugan, P.N. Barnes, G. Spanos, R.L. Holtz, Effects of nanoscale defects on critical current density of $(Y_{1-x}Eu_x)Ba_2Cu_3O_{7-\delta}$ thin films, Physica C 470 (2010) 318.

[4] F. Ben Azzouz, M. Zouaoui, A. Mellekh, M. Annabi, G. Van Tendeloo, M. Ben Salem, Flux pinning by Al-based nanoparticles embedded in YBCO: a transmission electron microscopic study, Physica C 455 (2007) 19.

[5] Y. Zhao, C.H. Chen, J. Wang, Flux pinning by NiO-induced nano-pinning centers in melt-textured YBCO superconductor, Supercond. Sci. Technol. 18 (2005) S43.

[6] J. Plain, T. Puig, F. Sandiumenge, X. Obradors, J. Rabier, Microstructural influence on critical currents and irreversibility line in melt-textured $YBa_2Cu_3O_{7-x}$ reannealed at high oxygen pressure, Phys. Rev. B: Condens. Matter 65 (2002) 104526.

[7] S.Y. Chen, I.G. Chen, Improvement to superconductivity using small amounts of Pd addition in Sm–Ba–Cu–O materials, Supercond. Sci. Technol. 17 (2004) 71.

[8] N. Hari Babu, E.S. Reddy, D.A. Cardwell, A.M. Campbell, C.D. Tarrant, K.R. Schneider, Artificial flux pinning centers in large, single-grain (RE) –Ba–Cu–O superconductors, Appl. Phys. Lett. 83 (2003) 4806.

[9] K. Nakashima, N. Chikumoto, A. Ibi, S. Miyata, Y. Yamada, T. Kubo, A. Suzuki, T. Terai, Effect of ion-irradiation and annealing on superconductive property of PLD prepared YBCO tapes, Physica C 463–465 (2007) 665.

[10] A. Hamrita, F. Ben Azzouz, W. Dachraoui, M. Ben Salem, The effect of silver inclusion on superconducting properties of $YBa_2Cu_3O_y$ prepared using planetary ball milling, J. Supercond. Nov. Magn. 26 (2013) 879.

[11] S. Patnaik, A. Gurevich, S.D Bu, S.D. Kaushik, J. Choi, C.B. Eom, D. C. Larbalestier, Thermally activated current transport in MgB_2 films, Phys. Rev. B: Condens. Matter 70 (2004) 064503.

[12] S. Dadras, Y. Liu, Y.S. Chai, V. Daadmehr, K.H. Kim, Increase of critical current density with doping carbon nano-tubes in $YBa_2Cu_3O_{7-\delta}$, Physica C 469 (2009) 55.

[13] M. Farbod, R.M. Batvandi, Doping effect of Ag nanoparticles on critical current of $YBa_2Cu_3O_{-\delta}$ bulk superconductor, Physica C 471 (2011) 112.

[14] I.E. Agranovski, Y. Ilyushechkin, I.S. Altman, T.E. Bostrom, M. Choi, Methods of introduction of MgO nanoparticles into Bi-2212/Ag tapes, Physica C 434 (2006) 115.

[15] A. Goyal, S. Kang, K.J. Leonard, P.M. Martin, A.A. Gapud, M. Varela, M. Paranthaman, A.O. Ijaduola, E.D. Specht, J.R. Thompson, D. K. Christen, S.J. Pennycook, F.A. List, Irradiation-free, columnar defects comprised of self-assembled nanodots and nanorods resulting in strongly enhanced flux-pinning in $YBa_2Cu_3O_{7-\delta}$ films, Supercond. Sci. Technol. 18 (2005) 1533.

[16] P. Mele, K. Matsumoto, T. Horide, A. Ichinose, M. Mukaida, Y. Y. Oshida, S. Horii, R. Kita, Ultra-high flux pinning properties of $BaMO_3$-doped $YBa_2Cu_3O_{7-x}$ thin films (M=Zr, Sn), Supercond. Sci. Technol. 21 (2008) 032002.

[17] K. Yamada, A. Ichinose, S. Horii, H. Kai, R. Teranishi, M. Mukaida, R. Kita, S. Kato, Y. Yoshida, K. Matsumoto, S. Toh, Characterization of nanorods in $BaNb_2O_6$-doped Er123 films revealed by cross-sectional transmission electron microscopy, Physica C 468 (2008) 1638.
[18] S.X. Dou, S. Soltanian, J. Horvat, X.L. Wang, H. Zhou, M. Ionescu, H. K. Liu, P. Munroe, M. Tomsic, Enhancement of the critical current density and flux pinning of MgB_2 superconductor by nanoparticle SiC doping, Appl. Phys. Lett. 81 (2002) 3419.
[19] A. Matsumoto, H. Kumakura, H. Kitaguchi, H. Hatakeyama, Effect of SiO_2 and SiC doping on the powder-in-tube processed MgB_2 tapes, Supercond. Sci. Technol. 16 (2003) 926.
[20] Y.C. Guo, Y. Tanaka, T. Kuroda, S.X. Dou, Z.Q. Yang, Addition of nanometer SiC in the silver-sheathed Bi2223 superconducting tapes, Physica C 311 (1999) 65.
[21] X.F. Rui, Y. Zhao, Y.Y. Xu, L. Zhang1, F.X. Sun, Y.Z. Wang, H. Zhang, Improved flux pinning behaviour in bulk MgB_2 achieved by nano-SiO_2 addition, Supercond. Sci. Technol. 17 (2004) 689.
[22] S.Y. Chen, P.C. Hseih, I.G. Chen, M.K. Wu, Effect of nano-scale additions on the superconductivity and pinning mechanism in the Sm–Ba–Cu–O materials, Chin. J. Phys. 43 (2005) 666.
[23] A.A. Khurram, I. Qasim, N. Khan, Si doped $(Cu_{0.5},Tl_{0.5})Ba_2Ca_2Cu_3O_{10-d}$ superconductors, J. Phys. Chem. Solids 72 (2011) 755.
[24] A. Kumar, J. Narayan, Superconducting $YBa_2Cu_3O_{7-d}$ thin films on Si (100) substrates with CoSi, buffer layers by an in situ pulsed laser evaporation method, Appl. Phys. Lett. 59 (1991) 1785.
[25] J Du, K.E Leslie, C.P Foley, G.L Harding, B. Sankrithyan, D.L. Tilbrook, Effects of sputtered SiO_2 passivation layers on YBCO microbridges and step-edge junctions, Supercond. Sci. Technol. 12 (1999) 1027.
[26] A. Gupta, A.J. Deshpande, V.P.S. Awana, S. Balamurugan, K.N. Sood, R. Kishore, H. Kishan, E. Takayama-Muromachi, A.V. Narlikar, Flux line motion in superconducting $(YBa_2Cu_3O_{7-d})_{1-x}/(SiO_2)_x$ composite systems in high magnetic fields, Supercond. Sci. Technol. 20 (2007) 1084.
[27] D. Dew-Hughes, Flux pinning mechanisms in type II superconductor, Philos. Mag. 30 (1974) 293.
[28] C.P. Bean, Magnetization of hard superconductors, Phys. Rev. Lett. 8 (1962) 250.
[29] R. Mohan, K. Singh, N. Kaur, S. Bhattacharya, M. Dixit, N.K. Gaur, V. Shelke, S.K. Gupta, R.K. Singh, Calcium and oxygen doping in Y $Ba_2Cu_3O_y$, Solid State Commun. 141 (2007) 605.
[30] Y. Zhu, Z.X. Cai, R.C. Budhani, M. Suenaga, D.O. Welch, Structures and effects of radiation damage in cuprate superconductors irradiated with several-hundred-MeV heavy ions, Phys. Rev. B: Condens. Matter 48 (1993) 6436.
[31] A.A. Gapud, D. Kumar, S.K. Viswanathan, C. Cantoni, M. Varela, J. Abiade, S.J. Pennycook, D.K. Christen, Enhancement of flux pinning in $YBa_2Cu_3O_{7-\delta}$ thin films embedded with epitaxially grown Y_2O_3 nanostructures using a multi-layering process, Supercond. Sci. Technol. 18 (2005) 1502.
[32] S.B. Guner, O. Gorur, S. Celik, M. Dogruer, G. Yildirim, A. Varilci, C. Terzioglu, Effect of zirconium diffusion on the microstructural and superconducting properties of $YBa_2Cu_3O_{7-\delta}$ superconductors, J. Alloys Compd 540 (2012) 260.
[33] E.K. Nazarova, A.J. Zaleski, K.A. Nenkov, A.L. Zahariev, Intergranular flux pinning in underdoped and overdoped $R_{1-x}Ca_xBa_2Cu_3O_z$ (R=Y, Gd; x=0, 0.2), Physica C 468 (2008) 955.
[34] K. Matsumoto, P. Mele, Artificial pinning center technology to enhance vortex pinning in YBCO coated conductors, Supercond. Sci. Technol. 23 (2010) 014001.
[35] L.M. Paulius, J.A. Fendrich, W.K. Kwok, A.E. Koshelev, V.M. Vinokur, G.W. Crabtree, B.G. Glagola, Effects of 1-GeV uranium ion irradiation on vortex pinning in single crystals of the high-temperature superconductor $YBa_2Cu_3O_{7-\delta}$, Phys. Rev. B: Condens. Matter 56 (1997) 913.
[36] X.U. Sheng, Y. Aiping, G.U. Yangni, W.U. Xiaoshan, Effect of Yb_2O_3 additives on structure and transport properties of $YBa_2Cu_3O_{7-\delta}$, J. Rare Earths 28 (2010) 434.
[37] G. Blatter, M. Feigel'man, V. Geshkenbein, A. Larkin, V. Vinokur, Vortices in high-temperature superconductors, Rev. Mod. Phys. 66 (1994) 1125.
[38] D.R. Nelson, V.M. Vinokur, Boson localization and correlated pinning of superconducting vortex arrays, Phys. Rev. B: Condens. Matter 48 (1993) 13060.
[39] B. Martinez, X. Obradors, A. Gou, V. Gomis, S. Pinol, J. Fontcuberta, H. Van Tol, Critical currents and pinning mechanisms in directionally solidified $YBa_2Cu_3O_7$-Y_2BaCuO_5 composites, Phys. Rev. B: Condens. Matter 53 (1996) 2797.